Extent and Energetics of the Hawaiian Lee Countercurrent

BY RICK LUMPKIN AND PIERRE J. FLAMENT

ABSTRACT. Direct velocity observations from drogued drifters in the Hawaiian Island region are used to map the time-mean and seasonal variability of the Hawaiian Lee Countercurrent (HLCC). The density of these data has more than doubled since the initial discovery of the HLCC. They provide valuable absolute estimates of HLCC velocity structure and variability, complementing data derived from geostrophy and numerical simulations. The data demonstrate that the HLCC has a peak annual mean velocity > 9 cm s^{-1}, with the strongest velocities along 19.75°N and eastward speeds in the longitudinal range 170°W to 157°W. The HLCC is relatively weak from March to May compared to its strength in other months. In the longitude band 160°–168°W, an eddy-to-mean energy flux of 3.3 ± 1.2 μW m^{-3} is found in the annual mean associated with the Reynolds shear stress, maintaining the shear between the HLCC and the North Equatorial Current to its south. This shear stress is associated with energetic anticyclonic eddies that are shed from the Big Island of Hawaii and propagate west-southwest. This energy flux is nearly twice as large during the peak HLCC months of August to January. It is sufficient to spin up the HLCC in O(10 days), and it is associated with an eddy spin-down time of O(100 days).

INTRODUCTION

The Hawaiian Island chain creates a barrier to large-scale westward oceanic and atmospheric flows, resulting in a complex wake that varies across a broad range of temporal and spatial scales. The major islands extend above the trade wind inversion layer, leading to sharply defined atmospheric shadows behind the major islands and atmospheric jets between them (Patzert, 1969; Chavanne et al., 2002). The island chain blocks the westward North Equatorial Current (NEC), creating an accelerated westward NEC jet at 17°–18°N to the west of the islands and also creating the North Hawaiian Ridge Current running west-northwest along the windward coasts of the islands (Qiu et al., 1997).

Westward-propagating energetic cyclonic and anticyclonic submesoscale to mesoscale eddies formed in the immediate lee of the Big Island of Hawaii dominate the oceanic lee of the Hawaiian Islands (Patzert, 1969; Lumpkin, 1998). The eddies' subsequent poleward (cyclonic) and equatorward (anticyclonic) drift added to their westward propagation creates broad regions of predominantly cyclonic vorticity north of ~ 19.5°N and anticyclonic vorticity south of 19.5°N (Lumpkin, 1998; Lumpkin and Flament, 2001). These eddies are forced by vortex shedding from the large-scale oceanic flow passing around the islands (McGary, 1955) and/or Ekman pumping associated with the islands' atmospheric wake (Patzert, 1968; Chavanne et al., 2002). Recent model studies (Jia et al., 2011; Kersalé et al., 2011) disagree on whether both mechanisms may be significant or if wind forcing alone can account for the eddies' presence.

At longer time scales, and consistent with the vorticity structure of these regions, the islands' oceanic wake is

characterized by a west-northwestward current along the lee coasts of the major Hawaiian Islands, called the Hawaiian Lee Current (HLC; Lumpkin, 1998), and a narrow countercurrent centered at ~ 19.5°N, called the Hawaiian Lee Countercurrent (HLCC). Flament (1993, 1994) named and first reported the HLCC from drifter observations as an eastward current extending from ~ 168°W to 157°W in the latitude range 19°–20°N (i.e., separating the mean pathways of cyclonic lee eddies to its north and anticyclonic lee eddies to its south). The westernmost limit of the HLCC was not well defined in Qiu et al. (1997) due to relatively sparse drifter data. The HLCC did not exist in their 2½ layer model, and they speculated that was because the wind forcing for the model did not include the fine structure of the atmospheric wake. They also speculated that there was a link between the oceanic lee vortices and the HLCC. The HLCC is believed to be forced by the Sverdrup response to the large-scale island atmospheric wake (White and Walker, 1985; Leonardi, 1998), which is a wind stress curl dipole (Chavanne et al., 2002). HLCC characteristics depend upon the fine-scale structure of this atmospheric wake. Sasaki and Nonaka (2006) found an HLCC in high-resolution (0.1°) model runs forced by both relatively smooth National Centers for Environmental Prediction/National Center for Atmospheric Research (NCEP/NCAR) reanalysis winds and high-resolution QuikSCAT-based winds. However, they noted that the HLCC was present over a much broader zonal range in the QuikSCAT run—extending from 170°E east-northeastward to the immediate lee of the Big Island—while it was only seen west of the dateline in the NCEP/NCAR run. They also noted that warm sea surface temperature (SST) anomalies advected by the HLCC had a distribution consistent with wind stress curl anomalies in the QuickSCAT fields, suggesting that the HLCC affects the wind field, and that these wind stress curl anomalies in turn act to reinforce the HLCC in a positive feedback. The HLCC exhibits variations in its strength and position at seasonal (Kobashi and Kawamura, 2002) to interannual (Yoshida et al., 2011) time scales in response to changes in the wind stress field.

The role of eddy fluxes in setting the zonal extent of the HLCC has been the subject of some debate in the literature. Qiu et al. (1997) found that the HLCC extended from ~ 168°W to 157°W in drifter observations, but the western limit was poorly resolved by those observations. Using drifter data through 1999, Yu et al. (2003) found an HLCC confined between 172°W and 158°W. In both a 1½ layer model and a primitive equation model forced by high-resolution winds, Xie et al. (2001) found that the HLCC extended from the Asian coast to the Hawaiian Islands. In a 2½ layer model, Yu et al. (2003) found that the HLCC did not exist west of ~ 175°W due to baroclinic instability, which fed a mean-to-eddy energy flux, and noted that the structure of the HLCC in numerical simulations can thus depend strongly on model resolution. Using drifter observations, Lumpkin (1998) calculated an eddy-to-mean barotropic energy conversion of 10 ± 8 μW m^{-3} at 18°–19°N averaged in the longitude band 160°–168°W (i.e., the location of the shear between the NEC and HLCC) associated with the Reynolds shear stress. This result suggests that eddy-to-mean conversion could be an additional significant source of energy for the HLCC. Yu et al. (2003) also examined barotropic energy conversion, averaging drifter observations collected through 1999 in the band 157°W to 172°W; however, in this broader band they found inconclusive results. Both Lumpkin (1998) and Yu et al. (2003) suffered from the relatively few drifter observations available in the pre-2000 time period, and both calculated time-mean currents by simple bin-averaging, a process that can potentially contaminate

> “IN THIS STUDY, ABSOLUTE CURRENTS AT 15 M DEPTH FROM DROGUED DRIFTERS WERE USED TO MAP THE EXTENT AND SEASONAL VARIABILITY OF THE [HAWAIIAN LEE COUNTERCURRENT].”

Rick Lumpkin *(rick.lumpkin@noaa.gov) is Oceanographer, National Oceanic and Atmospheric Administration/Atlantic Oceanographic and Meteorological Laboratory, Miami, FL, USA.* **Pierre J. Flament** *is Professor of Oceanography, University of Hawai'i at Manoa, Honolulu, HI, USA.*

eddy fluxes due to contamination by the mean shear (see Bauer et al., 1998).

It is worth noting that few studies of the HLCC have used direct velocity measurements, relying instead on geostrophy (e.g., Kobashi and Kawamura, 2002; Yoshida et al., 2011) or numerical models (e.g., Sasaki and Nonaka, 2006; Jia et al., 2011). Drifter data density in the Hawaiian Island region has approximately doubled since Qiu et al. (1997) and Lumpkin (1998). In this paper, we investigate the zonal extent of the HLCC and the magnitude and significance of barotropic energy conversion terms, using the modern set of drogued drifter observations, including post-1999 observations, to allow both better spatial resolution and resolution of seasonal variations.

DATA AND METHODS

This analysis uses quality-controlled drifter observations from 1979 through July 2012, interpolated to regular 6 h intervals (Hansen and Poulain, 1996). The drifters are Global Drifter Program-type, drogued at 15 m to follow mixed-layer currents (Niiler et al., 1995; Niiler, 2001; Lumpkin and Pazos, 2007). Zonal u and meridional v velocities are obtained every 6 h via 12 h centered differencing of the interpolated positions. Only data from drogued drifters are used, following results of a recent reevaluation of drogue presence based on anomalous downwind motion, submergence or tether strain, and transmission frequency anomalies (Lumpkin et al., 2013). Six-hour NCEP/NCAR Reanalysis 1 winds W are interpolated to the data and a downwind slip (motion with respect to the drogue depth of 15 m) of $7 \times 10^{-4}\, W$ (Niiler and Paduan, 1995) is removed from the drifter velocities. The Lagrangian time series of velocity for each drifter is then low-pass filtered at 5 d to remove tidal and near-inertial components of the flow, then decimated to daily values for this analysis. This 5 d low-pass filtering is performed without regard to geographic location, and reduces high-frequency changes in velocity. The resulting velocities contain all components of the total motion within the mixed layer at a depth of 15 m, including geostrophic and Ekman flow.

In the Hawaiian Island region (150°–180°W, 14°–25°N; Figure 1), 324 unique drifters have collected 130 drifter-years of velocity data, approximately twice the 64 drifter-years collected by 144 unique drifters available to Lumpkin (1998). Observational density is greatest in the immediate lee of the Hawaiian Islands where it exceeds 200 drifter-days per square degree. It is lowest south of 16°N and near the dateline, where density is fewer than 100 drifter-days per square degree in each region (Figure 1a). A single drifter collected the earliest drogued data in September 1980. Starting in January 1988, the number of drifters in the

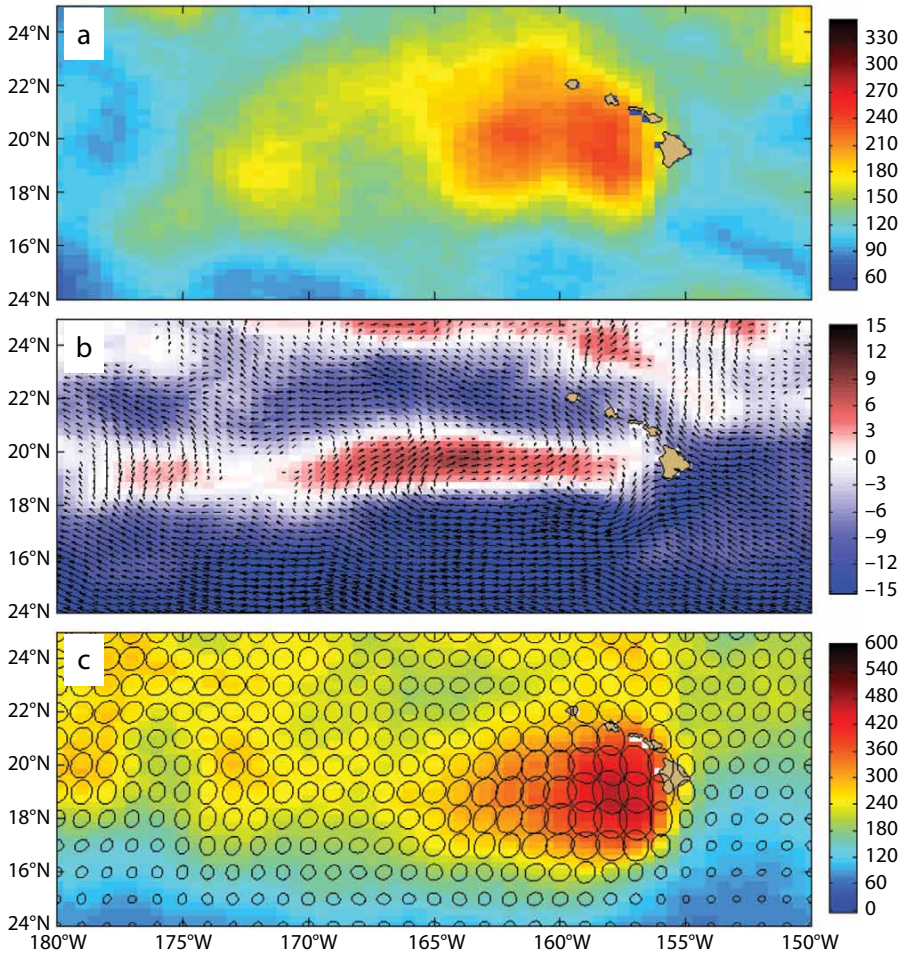

Figure 1. (a) Density of drogued drifter observations (drifter days per square degree). (b) Time-mean total near-surface currents (arrows) superimposed on mean zonal speed (colors; cm s^{-1}). Arrows not shown where magnitude is not significantly different from zero. (c) Eddy kinetic energy $\frac{1}{2}\langle u'^2 + v'^2 \rangle$ (colors indicate $cm^2\ s^{-2}$) and variance ellipses, shown on a 1° grid (a subset of the bins).

region grew relatively steadily until the end of 1991. Data density diminished from 1992 to mid-1994, then grew to its peak in 1995/96 thanks to deployments related to the World Ocean Circulation Experiment Surface Velocity Program and the Pelagic Fisheries Research Program (Lumpkin, 1998). Data density then diminished rapidly until it again spiked in 2000. It has remained relatively steady since 2005, with an average of 11.3 drogued drifters per year sampling the region.

Large-scale zonal U and meridional V drifter speeds were mapped in elliptical bins of constant area $\pi \times (2°)^2$, with orientation and eccentricity set by the variance ellipse within the bin (Johnson, 2001). This bin area was chosen subjectively to balance resolution of known current features while limiting aliased short-term variability in the Hawaiian Island region. The bin centers were chosen on a 0.5° × 0.25° longitude-latitude grid. Within each bin, drifter zonal and meridional speeds were decomposed into a time-mean, annual and semiannual sinusoids (Johnson, 2001; Lumpkin, 2003), spatial gradients up to second order polynomials (Bauer et al., 1998), and a term proportional to a five-month running mean of the Southern Oscillation Index (SOI; Johnson, 2001). This procedure was repeated five times in each bin (as in Johnson, 2001) to guarantee convergence of the bin shape, starting from a circular bin and refining the bin shape each iteration based on the variance ellipse of residuals within the bin. Coefficients for these components were determined via a Gauss-Markov approach that provides formal error bars (Lumpkin, 2003). More details on this methodology will soon be available based on recent work of author Lumpkin and Gregory Johnson of NOAA's Pacific Marine Environmental Laboratory (PMEL). We denote this mapping operator as $\langle\cdot\rangle$, for example, $U = \langle u \rangle$. Eddy velocities u', v' were calculated as the residuals in this fit (i.e., residuals not explained by seasonal and SOI-related variations and spatial gradients), such that $u' = u - U$, $v' = v - V$.

Ekman currents, driven by the northeasterly trade winds in the Hawaiian Island region, represent a significant fraction of the total motion measured by the 15 m-drogued drifters. To estimate their magnitude from the NCEP winds interpolated to the drifters, we used the Ralph and Niiler (1999) parameterization with updated coefficient from Niiler (2001).

RESULTS

Annual mean eddy kinetic energy $\frac{1}{2}\langle u'^2 + v'^2 \rangle$ (Figure 1c) reaches a local maximum in the immediate lee of the Hawaiian Islands, with values exceeding 400 cm^2 s^{-2}, associated with the formation region of lee cyclonic and anticyclonic eddies (Patzert, 1969; Lumpkin, 1998). The associated variance ellipses (Figure 1c), which determine the bins used to map the observations, exhibit some eccentricity in the lee of the islands, within and west of the area of maximum eddy kinetic energy. In this region, the variance ellipses tend to be tilted with semi-major axes oriented northeast-southwest.

In the drifter-derived time-mean field (Figure 1b), HLCC maximum velocities are located along 19.75°N. At this latitude, the eastward speed exceeds 8 cm s^{-1} in the longitude range 163°–165°W. The overall maximum time-mean eastward speed in the HLCC in total near-surface currents, 9.1 ± 1.3 cm s^{-1}, is found at 19.75°N, 164.00°W. The extent of the HLCC as defined by positive (eastward) velocities significantly different from zero in annual mean total near-surface currents is 170°W to 157°W; including eastward velocities not significantly different from zero expands the extent to 170.5°W to 156.0°W. From the dateline to 170.0°W, meridional speeds are significant and northward, but the zonal component of velocity is not; a band of eastward speeds of ~ 1.0 ± 1.5 cm s^{-1} is found at 177.5°W to 174.0°W, separated from the HLCC by a band of westward (but not significantly different from zero) speeds at 170.5°–174.0°W.

The Ekman component of the motion is generally toward the northwest, consistent with the northeasterly trade winds. The Ekman-removed currents thus exhibit a stronger HLCC, with a peak eastward speed of 18.1 ± 1.3 cm s^{-1} at 19.75°N, 163.00°W. This speed does not radically change the zonal extent of the HLCC: in Ekman-removed currents, eastward speeds significantly different from zero are found in the longitude band 157.5°–168.5°W along 19.75°N, with a separate band of significant eastward speeds at 173°–178°W. Seasonal variations of the HLCC can be reconstructed from the time mean coefficient and the annual and semiannual harmonic fit to the total current observations in each bin. This reconstruction (Figure 2) reveals that the HLCC exhibits both annual and semiannual fluctuations. The climatological monthly peak speed of the HLCC has a minimum of 5.3 ± 0.2 cm s^{-1} in April, rises to a maximum of 13.6 ± 0.3 cm s^{-1} in August, drops slightly to a relative minimum of 10.2 ± 0.2 cm s^{-1} in October, and then rises to a relative maximum of 13.2 ± 0.2 cm s^{-1} in January. This result is consistent with the seasonal variability

diagnosed from hydrographic casts and altimetry by Kobashi and Kawamura (2002), who found that the current was strongest in July to February and weakest in April to June. During late summer through fall, the western half of the HLCC shifts southward and extends further to the west (Figure 2) while the eastern half remains at 19.5°–20.0°N. In Ekman-removed currents (not shown), the seasonal cycle is qualitatively similar, with stronger eastward speeds seen in all months. As a consequence, the HLCC is more clearly present in Ekman-removed April currents than it is in total currents.

Figure 3 shows drifter-derived values averaged in the longitude band 160°–168°W. Standard error bars on U (Figure 3a), V (not shown), and eddy velocity variances and covariances $\langle u'^2 \rangle$, $\langle v'^2 \rangle$, and $\langle u'v' \rangle$ are formal errors derived in the Gauss-Markov inversion (Lumpkin, 2003; recent work of author Lumpkin and Gregory Johnson of PMEL). In Figure 3, the dashed curves are for the annual mean total currents, while the solid curves with error bars are for the months of peak HLCC, August through January. The dotted curves are the annual mean Ekman-removed currents, representing the predominantly geostrophic currents beneath the surface mixed layer. In all three curves, the eddy velocity covariance terms $\langle u'^2 \rangle$ and $\langle v'^2 \rangle$ are similar (not shown) in the HLCC region, with an eddy kinetic energy peak of 290–300 $m^2\ s^{-2}$ at 17°–21°N (Figure 3b). The Reynolds shear stress $\langle u'v' \rangle$ is not significantly different from zero at the northern edge of the HLCC, but increases to significantly positive values that peak at ~ 18°N. In the annual mean total (Figure 3c, dashed), the Reynolds shear stress reaches a maximum of 25.7 ± 3.0 $cm^2\ s^{-2}$ at 18.25°N. This change over a meridional scale of O(100 km) suggests an eastward acceleration of ~ 2×10^{-8} $m\ s^{-2}$, approximately two orders of magnitude smaller than fU ~ 3×10^{-6} $m\ s^{-2}$ and consistent with an HLCC spin-up time of ~ (7 $cm\ s^{-1}$)/(2×10^{-8} $m\ s^{-2}$) = ~ 40 days. However, this estimate neglects the fact that the Reynolds shear stress is acting in the presence of a sharp meridional gradient in U; derived below, the energy flux associated with the resulting barotropic instability implies a significantly faster spin-up time.

As noted in the introduction, there is controversy in the literature regarding the significance of barotropic instability in the energy balance of the HLCC. Several terms in the turbulent energy equation can be derived from drifter observations (see Hansen and Paul, 1984). This equation can be written

$$\rho_0 \frac{d}{dt}\left(\left\langle u'^2 \right\rangle + \left\langle v'^2 \right\rangle\right) =$$

$$-\rho_0 \left\langle u'v' \right\rangle \left(\partial_y U - \partial_x V\right) - \rho_0 \left\langle u'^2 \right\rangle \partial_x U$$

$$-\rho_0 \left\langle v'^2 \right\rangle \partial_y V + \ldots$$

where the left-hand side is the rate of change of eddy kinetic energy and the right-hand side contains barotropic instability terms related to fluxes of energy between the mean and eddy components of the flow, associated with time-mean eddy advection across mean flow gradients. Additional terms in the overall eddy energy equation

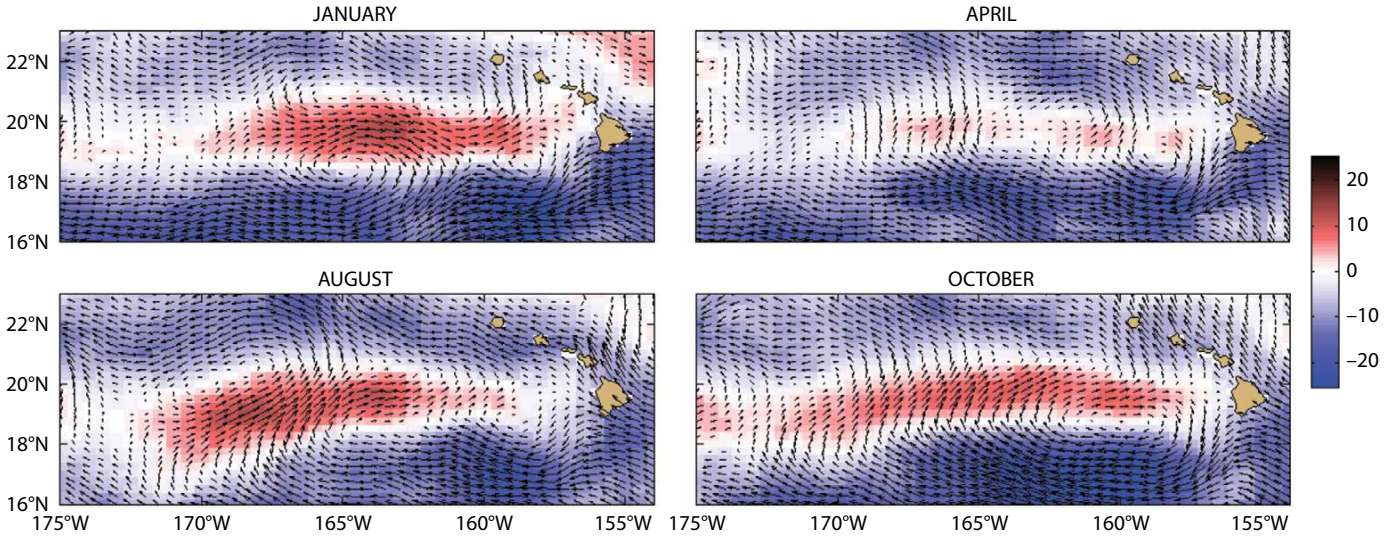

Figure 2. Climatological monthly mean total near-surface currents (arrows) superimposed on zonal speed (colors indicate cm s^{-1}) for January (top left), April (top right), August (bottom left), and October (bottom right). Arrows are not shown where magnitude is not significantly different from zero.

(see Hansen and Paul, 1984) are related to potential energy and baroclinic instability, and require measurements or estimates of vertical density gradients and density anomalies concurrent with the eddy velocities. A positive value in the left-hand side is an increase of eddy kinetic energy (i.e., mean-to-eddy energy flux), while negative values indicate eddy-to-mean energy flux.

In Figure 3, errors in the gradients of U and V are calculated from the formal error bars in U and V, assuming that errors are uncorrelated from one latitude bin to the next. In the longitude band 160°–168°W, the zonal gradient of U and meridional gradient of V are small. These terms combine with the relatively large Reynolds normal stress terms $\langle u'^2 \rangle$ and $\langle v'^2 \rangle$ (sum shown in Figure 3b; south of 22.75°N, these terms differ by < 20 cm^2 s^{-2}), respectively, to yield two of the mean-to-eddy barotropic energy conversion terms. The results (Figure 3d,e) are relatively large energy fluxes, but with large associated standard errors; at no latitude in the longitude band 160°–168°W are they significantly different from zero. More observations are needed to reduce these error estimates and to determine the significance of these terms.

In contrast, one of the terms associated with the Reynolds shear stress $\langle u'v' \rangle$ (Figure 3c) is significant (Lumpkin, 1998). South of the HLCC, where anticyclonic vorticity dominates the oceanic wake of the Hawaiian Islands (Lumpkin and Flament, 2001), the annual mean total zonal speed U averaged in the band 160°–168°W (Figure 3a, dashed curve) goes from –10.2 cm s^{-1} at 18.0°N to 6.8 cm s^{-1} at 19.5°N, a mean gradient of 1.0×10^{-6} s^{-1}. The Reynolds shear stress $\langle u'v' \rangle$ works to reinforce this gradient, reaching a maximum of 25.7 ± 3.0 cm^2 s^{-2} at 18.25°N (Figure 3c, dashed curve). The associated energy flux $-\rho_0 \langle u'v' \rangle \partial U/\partial y$ reaches a minimum of –3.3 ± 1.2 μW m^{-3} at 18.25°N (assuming ρ_0 = 1,023 kg m^{-3}; Figure 3f, dashed curve) with the sign indicating an eddy-to-mean energy flux. This result indicates that the energetic anticyclonic lee eddies advect and deposit zonal momentum that maintains the meridional shear between the HLCC and the NEC to its south. In August through January, the peak months of the HLCC (Figure 2), the Reynolds shear stress increases to $\langle u'v' \rangle$ = 39.5 ± 3.6 cm^2 s^{-2} at 18.25°N (Figure 3c, solid curve), and the energy flux reaches a minimum of –6.1 ± 2.1 μW m^{-3} at 18.25°N (Figure 3f, solid curve). North of the northern edge of the HLCC, the Reynolds stress and associated energy flux are not significantly different from zero (Figure 3c, dashed curve). The term $-\rho_0 \langle u'v' \rangle \partial V/\partial x$ is small and not significantly different from zero, with a maximum amplitude of 0.1 ± 2.9 μW m^{-3} at 20°N in the annual mean (not shown). If the drifter observations are averaged in the longitudinal range 157°–172°W, as done by Yu et al. (2003), the results are qualitatively consistent; averaged in this band, the annual mean Reynolds shear stress peaks at 13.8 ± 2.2 cm^2 s^{-2},

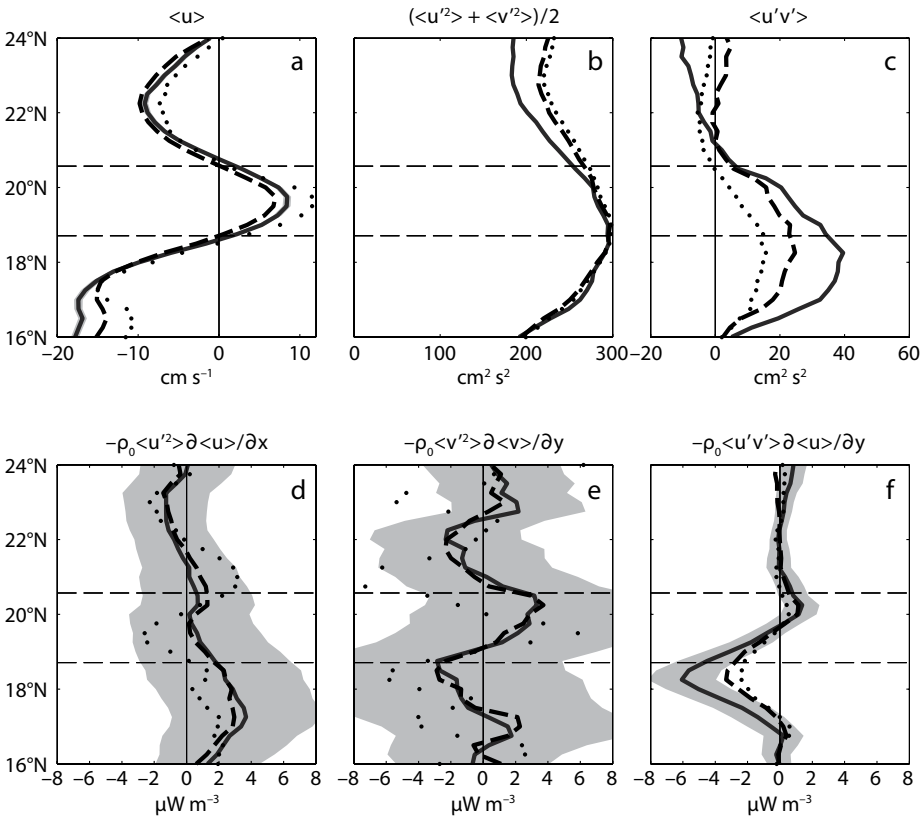

Figure 3. Drifter observations averaged in the longitude band 160°–168°W as a function of latitude. Horizontal dashed lines indicate the northern and southern edges of the HLCC. Dashed curves are the annual mean total currents; solid curves with shaded standard error bars are for the period August to January (the peak months of the HLCC); dots indicate annual mean values for the Ekman-removed currents. (a) Zonal velocity $\langle U \rangle$. (b) Eddy kinetic energy $\frac{1}{2}\langle u'^2 + v'^2 \rangle$. (c) Reynolds shear stress $\langle u'v' \rangle$. (d) Energy conversion term $-\rho_0 \langle v'^2 \rangle \partial V/\partial y$. (e) Energy conversion term $-\rho_0 \langle u'^2 \rangle \partial U/\partial x$. (f) Energy conversion term $-\rho_0 \langle u'v' \rangle \partial U/\partial y$.

and the annual-averaged eddy-to-mean energy flux $-\rho_0 \langle u'v' \rangle \partial U/\partial y$ peaks at 1.6 ± 0.7 μW m^{-3}, or 27.2 ± 1.2 cm^2 s^{-2} and 3.7 ± 1.3 μW m^{-3}, respectively, during the peak HLCC months. In Ekman-removed currents (Figure 3, dotted curves), the stronger meridional gradient in U is offset by a weaker Reynolds flux to yield a slightly weaker (by ~ 1 μW m^{-3}) eddy-to-mean energy flux associated with the Reynolds shear stress.

West of the HLCC, in the band 170°–180°W, the zonal velocity has an eastward maximum of 0.9 cm s^{-1} at 19°N in the total annual mean, peaking to 1.9 cm s^{-1} from August to November (not shown). In this longitude band, the kinetic energy flux is considerably smaller due to the reduced gradient of the mean zonal current. The annually averaged Reynolds shear stress $\langle u'v' \rangle$ reaches a maximum of 14.6 ± 2.6 cm^{-2} s^{-2} at 19°N in the longitude band 170°–180°W, approximately half its value in 160°–168°W, yielding a kinetic energy flux of -0.8 ± 0.5 μW m^{-3} (eddy-to-mean flux) at 18°N. During the peak HLCC months of August to January, these values increase to $\langle u'v' \rangle = 31.7 \pm 2.5$ cm^{-2} s^{-2} at 18°N and an energy flux of -1.8 ± 1.3 μW m^{-3} at 17.75°N.

DISCUSSION

As noted in the introduction, a number of estimates of the HLCC extent have appeared in the literature, with relatively few coming from direct velocity observations. In this study, absolute currents at 15 m depth from drogued drifters were used to map the extent and seasonal variability of the HLCC. Our results indicate an HLCC with a zonal extent consistent with earlier estimates of ~ 170°W to ~ 158°W (Qiu et al., 1997). We find significant eastward total velocities in the longitude range 170°W to 157°W, with another band of eastward velocity not significantly different from zero extending as far west as 177.5°W (Figure 1). The direct velocity measurements indicate that the current is relatively weak from March to May compared to its strength in other months, confirming results derived from geostrophy (Kobashi and Kawamura, 2002).

A number of studies (e.g., White and Walker, 1985; Leonardi, 1998; Chavanne et al., 2002; Sasaki and Nonaka, 2006) have demonstrated the significance of Sverdrup dynamics in setting the structure of the HLCC. In this study, we show that an additional component, the eddy-to-mean conversion of barotropic kinetic energy driven by lee vortices via the Reynolds shear stress, plays a significant role in HLCC energetics. This term was first estimated from drifter observations by Lumpkin (1998), who calculated a maximum eddy-to-mean value of 10 ± 8 μW m^{-3} between the HLCC and the NEC to its south in the annual mean. Here we find 3.3 ± 1.2 μW m^{-3} at 18.25°N in the annual mean, increasing to 6.1 ± 2.1 μW m^{-3} when averaged in the peak HLCC months of August to January. Perhaps coincidentally, Lumpkin (1998) estimated the spin-down rate of two well-sampled lee anticyclonic eddies at ~ 3 μW m^{-3} in the longitude range of the HLCC, consistent with our eddy-to-mean barotropic conversion rate. This energy flux is significant: if acting in isolation, it could spin up an HLCC of speed $U = 7$ cm s^{-1} in time $T = \rho_0 U^2/(2 \times [3\ \mu\text{W m}^{-3}]) =$ ~ 10 days, and during peak HLCC months ($U = 8.5$ cm s^{-1}, 160°–168°W average; Figure 3a) in seven days. It is unclear from this analysis what role baroclinic conversion may be playing in the mean energy balance, and more observations are needed to quantify the significance of barotropic conversion terms associated with the Reynolds normal stress. Regardless, these observations suggest that the Reynolds shear stress cannot be neglected in the HLCC. This flux, drawn from an eddy field of kinetic energy ~ 300 cm^2 s^{-2} (Figure 3b), suggests an eddy spin-down time of ~ 100 days in the absence of other significant fluxes. It is also possible that this energy flux is associated with an increase in potential energy at the expense of kinetic energy as eddies grow from small, newly formed, high Rossby number vortices in the immediate lee of the Big Island of Hawaii to quasigeostrophic eddies. However, at least one study (Flament et al., 2001) has examined the growth of the anticyclonic lee vortices as they merge downstream from their generation region; by the time that they reach the longitude band of the HLCC, Flament et al. (2001) suggest that they are low Rossby number, potential energy-dominated eddies. It is of course critical to remind the reader that the total energy budget of the HLCC includes baroclinic conversion terms not considered here, which likely represent a mean-to-eddy flux that counters the barotropic eddy-to-mean conversion in the HLCC. Examining the total energy balance in observations that can characterize all the relevant energy budget terms remains an important goal for future studies. Further to the west, model results suggest that mean-to-eddy baroclinic instability terms dominate the energy budget, limiting the western extent of the HLCC (Yu et al., 2003). In this region, we still find an eddy-to-mean

flux of energy from barotropic conversion, but it is much weaker than in the core longitude band of the HLCC.

ACKNOWLEDGMENTS

The authors would like to thank Verena Hormann, Renellys Perez, and two anonymous reviewers for valuable comments and suggestions for this paper. RL received support from NOAA's Climate Program Office and Atlantic Oceanographic and Meteorological Laboratory. PF receives support from NOAA's Integrated Ocean Observing System program and from the State of Hawaii. The drifter data were collected and made freely available by the Global Drifter Program (http://www.aoml.noaa.gov/phod/dac). NCEP Reanalysis data were provided by the NOAA-CIRES Climate Diagnostics Center, Boulder, CO (http://www.cdc.noaa.gov). University of Hawaii's School of Ocean and Earth Science and Technology (SOEST) contribution no. 8820.

REFERENCES

Bauer, S., M.S. Swenson, A. Griffa, A.J. Mariano, and K. Owens. 1998. Eddy–mean flow decomposition and eddy-diffusivity estimates in the tropical Pacific Ocean: 1. Methodology. *Journal of Geophysical Research* 103 (C13):30,855–30,871, http://dx.doi.org/10.1029/1998JC900009.

Chavanne, C., P. Flament, R. Lumpkin, B. Dousset, and A. Bentamy. 2002. Scatterometer observations of wind variations induced by oceanic islands: Implications for wind-driven ocean circulation. *Canadian Journal of Remote Sensing* 28:466–474.

Flament, P. 1993. Wind-driven mesoscale oceanic processes in the lee of the Hawaiian Islands. Proceedings of the third scientific meeting of The Oceanography Society, Seattle, WA (abstract only).

Flament, P. 1994. Wind-driven oceanic processes in the lee of the island of Hawaii. *Annales Geophysicae*. European Geophysical Society, Grenoble, C-268 (abstract only).

Flament, P., R. Lumpkin, J. Tournadre, and L. Armi. 2001. Vortex pairing in an unstable anticyclonic shear flow: Discrete subharmonics of one pendulum day. *Journal of Fluid Mechanics* 440:401–409, http://dx.doi.org/10.1017/S0022112001004955.

Hansen, D., and C.A. Paul. 1984. Genesis and effects of long waves in the equatorial Pacific. *Journal of Geophysical Research* 89:10,431–10,440, http://dx.doi.org/10.1029/JC089iC06p10431.

Hansen, D., and P.-M. Poulain. 1996. Quality control and interpolations of WOCE-TOGA drifter data. *Journal of Atmospheric and Oceanic Technology* 13:900–909, http://dx.doi.org/10.1175/1520-0426(1996)013<0900:QCAIOW>2.0.CO;2.

Jia, Y., P.H.R. Calil, E.P. Chassignet, E.J. Metzger, J.T. Potemra, K.J. Richards, and A.J. Wallcraft. 2011. Generation of mesoscale eddies in the lee of the Hawaiian Islands. *Journal of Geophysical Research* 116, C11009, http://dx.doi.org/10.1029/2011JC007305.

Johnson, G.C. 2001. The Pacific Ocean subtropical cell surface limb. *Geophysical Research Letters* 28:1,771–1,774, http://dx.doi.org/10.1029/2000GL012723.

Kersalé, M., A.M. Doglioli, and A.A. Petrenko. 2011. Sensitivity study of the generation of mesoscale eddies in a numerical model of the Hawaii islands. *Ocean Science* 7:277–291, http://dx.doi.org/10.5194/os-7-277-2011.

Kobashi, F., and H. Kawamura. 2002. Seasonal variation and instability nature of the North Pacific Subtropical Countercurrent and the Hawaiian Lee Countercurrent. *Journal of Geophysical Research* 107(C11), 3185, http://dx.doi.org/10.1029/2001JC001225.

Leonardi, A.P. 1998. Dynamics of the North Hawaiian Ridge Current. Master's thesis, College of Arts and Sciences, Florida State University.

Lumpkin, R. 1998. Eddies and currents of the Hawaiian Islands. PhD dissertation, University of Hawaii at Manoa.

Lumpkin, R., and P. Flament. 2001. Lagrangian statistics in the central North Pacific. *Journal of Marine Systems* 29:141–155, http://dx.doi.org/10.1016/S0924-7963(01)00014-8.

Lumpkin, R. 2003. Decomposition of surface drifter observations in the Atlantic Ocean. *Geophysical Research Letters* 30, 1753, http://dx.doi.org/10.1029/2003GL017519.

Lumpkin, R., and M. Pazos. 2007. Measuring surface currents with Surface Velocity Program drifters: The instrument, its data and some recent results. Pp. 39–67 in *Lagrangian Analysis and Prediction of Coastal and Ocean Dynamics*. A. Griffa, A.D. Kirwan, A. Mariano, T. Özgökmen, and T. Rossby, eds, Cambridge University Press.

Lumpkin, R., S. Grodsky, L. Centurioni, M.-H. Rio, J. Carton, and D. Lee. 2013. Removing spurious low-frequency variability in drifter velocities. *Journal of Atmospheric and Oceanic Technology* 30(2):353–360, http://dx.doi.org/10.1175/JTECH-D-12-00139.1.

McGary, J.W. 1955. *Mid-Pacific Oceanography, Part VI: Hawaiian Offshore Waters: December 1949–November 1951*. Technical Report 152, U.S. Fish and Wildlife Service, Special Science Report.

Niiler, P.P. 2001. The world ocean surface circulation. Pp. 193–204 in *Ocean Circulation and Climate: Observing and Modelling the Global Ocean*. G. Siedler, J. Church, and J. Gould, eds, International Geophysics Series, vol. *77*, Academic Press.

Niiler, P.P., and J.D. Paduan. 1995. Wind-driven motions in the northeast Pacific as measured by Lagrangian drifters. *Journal of Physical Oceanography* 25:2,819–2,830, http://dx.doi.org/10.1175/1520-0485(1995)025<2819:WDMITN>2.0.CO;2.

Niiler, P.P., A. Sybrandy, K. Bi, P. Poulain, and D. Bitterman. 1995. Measurements of the water-following capability of holey-sock and TRISTAR drifters. *Deep Sea Research Part I* 42:1,951–1,964, http://dx.doi.org/10.1016/0967-0637(95)00076-3.

Patzert, W.C. 1969. *Eddies in Hawaiian Waters*. Hawaii Institute of Geophysics Report 69-8, 51 pp.

Qiu, B., D. Koh, R. Lumpkin, and P. Flament. 1997. Existence and formation mechanism of the North Hawaiian Ridge Current. *Journal of Physical Oceanography* 27:431–444, http://dx.doi.org/10.1175/1520-0485(1997)027<0431:EAFMOT>2.0.CO;2.

Ralph, E.A., and P.P. Niiler. 1999. Wind-driven currents in the Tropical Pacific. *Journal of Physical Oceanography* 29:2,121–2,129, http://dx.doi.org/10.1175/1520-0485(1999)029<2121:WDCITT>2.0.CO;2.

Sasaki, H., and M. Nonaka. 2006. Far-reaching Hawaiian Lee Countercurrent driven by wind-stress curl induced by warm SST band along the current. *Geophysical Research Letters* 33, L13602, http://dx.doi.org/10.1029/2006GL026540.

White, W.B., and A.E. Walker. 1985. The influence of the Hawaiian Archipelago upon the wind-driven subtropical gyre of the western North Pacific. *Journal of Geophysical Research* 90:7,061–7,074, http://dx.doi.org/10.1029/JC090iC04p07061.

Xie, S.-P., W.T. Liu, Q. Liu, and M. Nonaka. 2001. Far-reaching effects of the Hawaiian Islands on the Pacific ocean-atmosphere system. *Science* 292:2,057–2,060, http://dx.doi.org/10.1126/science.1059781.

Yoshida, S., B. Qiu, and P. Hacker. 2011. Low-frequency eddy modulations in the Hawaiian Lee Countercurrent: Observations and connection to the Pacific Decadal Oscillation. *Journal of Geophysical Research* 116, C12009, http://dx.doi.org/10.1029/2011JC007286.

Yu, Z., N. Maximenko, S.-P. Xie, and M. Nonaka. 2003. On the termination of the Hawaiian Lee Countercurrent. *Geophysical Research Letters* 30, 1215, http://dx.doi.org/10.1029/2002GL016710.